Photoactivity of Dopped TiO_2 Thin Films by Ion Sputter Deposition

A. Gjevori[a,*] and B. Ziberi[b]

[a] *Physics Engineering Department, Polytechnic University of Tirana, Mother Theresa Square 4, 1000, Tirana, Albania*
[b] *Physics Department, University of Tetova, Ilinden Street nn, 1200, Tetova, Republic of North Macedonia*

Received: 30.04.2023 & Accepted: 20.07.2023

Doi: 10.12693/APhysPolA.144.144 *e-mail: a.gjevori@fimif.edu.al

Titanium dioxide is well known as a photoactive material to be activated under ultraviolet irradiation and is either employed as a photocatalyst or exhibits superhydrophilic behavior after reducing the surface energy under illumination for self-cleaning or anti-fogging surfaces. For increasing the reactivity of the thin films under solar illumination, a reduced band gap is desired. Doping with transition metals or with nitrogen has been reported in the literature. However, the incorporation of nitrogen into the growing film is a much more complex process, which is presently not completely understood. TiO_2 thin layers were produced by ion beam sputter deposition, which should allow the usage of temperature-sensitive substrates. The deposition has been performed in the existing experimental setup, previously used for investigations on Ag and Ge thin film physical vapor deposition processes, where the influence of the sputtered and reflected particles and their accompanying energy flux on the grain size, surface morphology, and conductivity have been measured. By adjusting the geometry between the incident ion beam, the sputter target, and the substrate, independently from the primary ion energy and species, a controlled deposition of samples was possible. Conventional ion implantation was employed to implant either carbon or nitrogen ions below the surface for bandgap engineering. The resulting thin films have subsequently been investigated for optical properties, stoichiometry, structural properties, surface topography, and photoactivity. The aim was to find an optimized geometry and to determine the exact particle and energy flux necessary for these conditions. Thus, the process opens up for transfer or scaling when assuming future industrial applications.

topics: ion beam sputter deposition, energy selective mass spectrometry, doping, surface energy

1. Introduction

Titanium dioxide is well known as a photoactive material to be activated under ultraviolet (UV) irradiation [1, 2] and is either employed as a photocatalyst or exhibits superhydrophilic behavior after reducing the surface energy under illumination for self-cleaning or anti-fogging surfaces [3]. As an alternative to powders, TiO_2 can be produced as thin films using chemical sol–gel processes operating in air or physical vapor deposition (PVD) processes, where either high temperature or increased ion energy is necessary to obtain the photoactive phase [4]. Even coating of membranes is possible using a more complex process [5]. There, temperature-sensitive substrates require low temperatures, ideally close to room temperature, where an amorphous photoactive phase can be formed under certain conditions [6, 7].

Regardless of the phase composition, the band gap is always more than 3 eV (the exact value depending on the polymorph), thus necessitating UV-A radiation for activation. For increasing the reactivity of thin films under solar illumination, a reduced band gap is desired. Doping with transition metals or with nitrogen has been reported in the literature [8, 9]. The latter dopant is — theoretically — readily accessible during PVD processes. However, the incorporation of nitrogen into the growing film, in contrast to the implantation of ions into TiO_2 thin films or selective oxidation of TiN, is a much more complex process that is presently not completely understood [10]. Alternatively, TiO_2 nanotubes with a reduced band gap [11], visible-light-active N-doped TiO_2 nanorods by hydrothermal treatment [12], or hydrazine doping of brookite nanorods at 200°C for 18 h have recently been proposed [13]. Despite the large amount of published work, even the photoactivity of pure titanium dioxide TiO_2 thin films is still a matter of controversy.

Therefore, an experiment was set up that offers the opportunity of reducing the bandgap of TiO_2 thin films, which increases the surface energy, leading to improved photoactive properties. TiO_2 thin films are produced by ion sputter deposition.

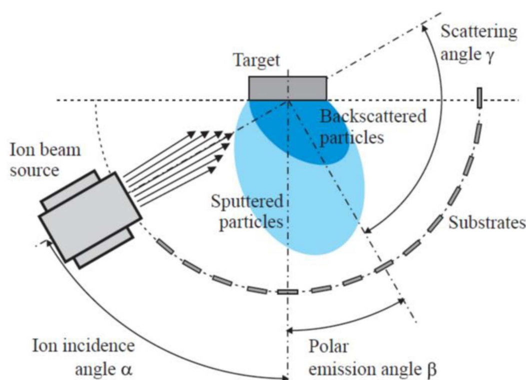

Fig. 1. Sketch of the IBSD experimental setup.

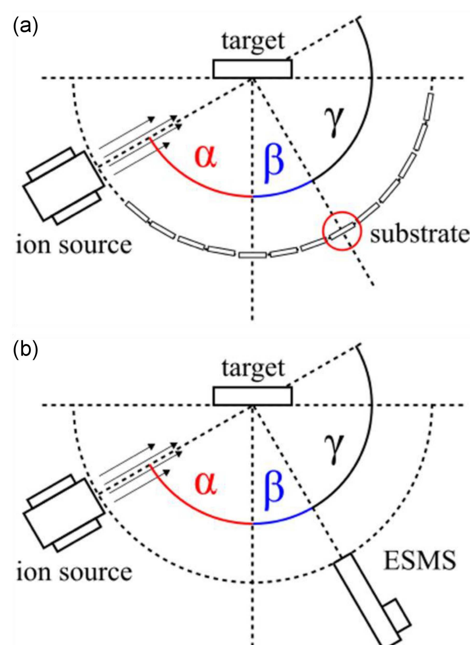

Fig. 2. Setup for deposition and ESMS measurements with the same geometry (Ti target + 2 sccm O_2).

Then, we employed mixtures of energies/species: 65 keV C + 75 keV N, 30 keV C + 35 keV N, and 35 keV N + 75 keV N to increase the local dopant concentration and to adjust the depth to the penetration range of the light. The purpose was to investigate whether synergy effects exist for a combination of carbon and nitrogen dopants. It was found that the ion implantation at concentrations less than 10 at.% can lead to increased photoactivity under UV illumination. Reducing the bandgap by carbon and/or nitrogen implantation before changing from semiconductor to semimetal is challenging. This was known for direct co-deposition during PVD by vacuum arc, and now it was shown to be also true for post-implantation after ion beam sputter deposition.

2. Experimental part

The samples are produced by ion beam sputter deposition (IBSD). Figure 1 shows a schematic sketch of the IBSD setup inside the deposition chamber [14]. It consists of a broad beam ion source, a target holder, and a substrate holder. The ion beam source and the target holder are placed on rotary tables, which have their center of rotation at the center of the target surface plane. Additionally, an energy-selective mass spectrometer was used to measure the energy distribution of sputtered target ions and backscattered primary ions. The deposition chamber is rectangular in shape with a dimension of $1 \times 1 \times 0.7$ m^3. The chamber was pumped by a 2200 l/s turbo molecular pump to a base pressure of 2×10^{-6} mbar. The working pressure during sputtering was about 7×10^{-5} mbar. The ion beam source is a radio frequency (RF) type with a three-grid multi-aperture extraction system with an open diameter of 16 mm. The ion incidence angle was fixed at 60°. The process gas was Ar with a volumetric flow rate of 3.5 sccm. The power of the 13.56 MHz RF plasma source was set to 70 W. The distance between the exit plane of the ion beam source and the target center is about 0.15 m, i.e., much smaller than the mean free path length of the primary ions (Ar — 1.28 m). The substrate holder is semi-circular in shape, with a radius of curvature of 0.15 m. The holder is segmented so that substrates can be placed at different polar emission angles in steps of 10°. TiO_2 thin films were grown under a variation of ion incidence angle, with an ion energy of 1 keV. Silicon (100) coupons with a size of about 15×25 mm^2 were used as the substrate material. A poly-crystalline Ti target with a purity of 99.99% was used. The deposition was done in an oxygen atmosphere with an oxygen volumetric flow rate of 2 sccm. The total deposition time was 6 h.

TiO_2 thin films were characterized in terms of mass density, film thickness, stoichiometry, structural properties, surface roughness, optical properties, and photoactivity.

The energy selective mass spectrometer (ESMS) Balzers Quadstar PPM 422 was used for measuring the mass distribution of secondary ions and the energy distribution of individual ion species (see Fig. 2). The mass ranges from 1 up to 512 amu with a resolution of 1 amu. The energy range is from 0 up to 500 eV with a resolution of 0.5 eV. Different combinations of the incidence angle α and the emission angle β can be realized by rotating the target and/or the ion source. The minimal detectable emission angle is limited by the geometrical dimensions of the ESMS and the ion source. An incidence angle of 60° results in a minimal emission angle of 0°. The energy distribution of sputtered ions (Ti, TiO, and O), backscattered ions (Ar), and O_2

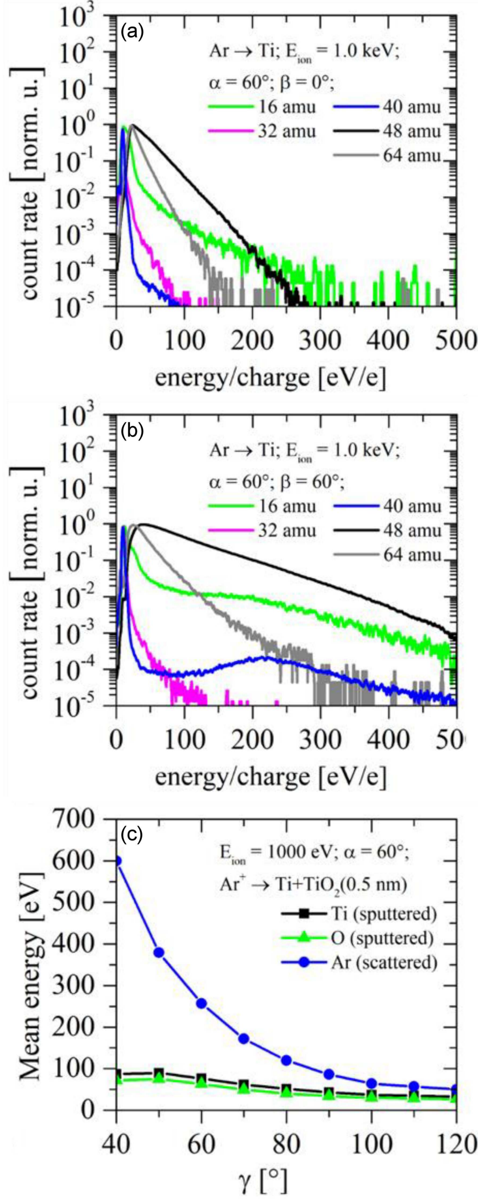

Fig. 3. Measured energy distributions of Ti ions sputtered from a polycrystalline Ti target under Ar ion bombardment with steady oxygen flow.

ions was measured at emission angles in steps of 10° for primary ion energy of 1.0 keV and incidence angle of 60°. The measured energy distributions were smoothed by the method of moving average with the average of over 50 adjacent data points [15].

Spectroscopic ellipsometry (SE) measurements are used for determining the film thickness and the band gap energy. Spectra of the ellipsometric parameters Ψ and Δ were measured in the photon energy range from $E_p = 0.73$ eV to $E_p = 6.4$ eV at six angles of incidence (50°, 55°, 60°, 65°, 70° and 75°) with an ellipsometer RC2-DI of dual-rotating-compensator type. The measured spectra were modeled using the Tauc–Lorentz (TL) model [15].

Rutherford backscattering spectrometry (RBS) measurements were performed in order to investigate the stoichiometry of TiO_2 thin films. Measurements were done with singly charged He ions with an energy of 2 MeV at the LIPSION facility [16].

Structural analysis of the samples was done by X-ray diffraction (XRD). For this purpose, a diffractometer Ultima IV Type III, Rigaku, was used. It is equipped with a Cu anode X-ray tube, a graded multilayer mirror (to obtain a parallel beam), a theta–theta goniometer, a parallel slit analyzer, and a scintillation detector.

The surface topography was measured by atomic force microscopy (AFM) with a large sample scanning force microscope from Bruker (Dimension Icon©). The device was operated in tapping mode (TM) and in a xy-closed loop configuration. The z-sensor signal is utilized for measuring the surface topography. Measurements were performed in air using silicon probes with a nominal tip radius of less than 5 nm. A scan size of 2×2 μm^2 with a resolution of 1024×1024 pixels was used. A detailed description of the AFM method used to analyze samples is given elsewhere [15].

The surface energy was derived from contact angle measurements with the data analysis according to the Owens–Wendt method [17]. Contact angle measurements on TiO_2 samples were performed using a Krüss contact angle measuring system G2, and the results have been obtained from the software DSA II (drop shape analysis II). In the dynamic contact angle measurements (CAM) mode, two different liquids are used, i.e., deionized water and ethylene glycol, employing manual drop position on the surface with 2–4 drops (because of the high wettability of the surface of the samples after UV irradiation). From each liquid with a start-volume of 3 μl and end-volume of 4 μl, 10 successive snapshots were taken for each drop.

Photoactivity was examined by exposing the samples to UV-A light, generated from an actinic tube in the spectral range of 300–460 nm and with the maximum at 365 nm, at an intensity of 1 mW/cm^2, for up to 3 h.

Then the samples are doped with carbon and nitrogen using a conventional ion implanter IMC-200. The aim was to reduce the band gap of the UV-active TiO_2 thin films, as well as to investigate the effect of implantation on non-photoactive TiO_2 thin films. The following implantation parameters were used: energies for C^+ ions — 30 keV and 65 keV, energies for N^+ ions — 35 keV and 75 keV, average implantation time — 35 min, and total fluence — 2×10^{16} cm^{-2}.

3. Results and discussions

From the measurements of the mass distribution of secondary ions and the energy distribution of individual ion species, we observe that the predominant secondary ion species are: O^+ (16 amu),

TABLE I

TiO_2 film thickness as measured by ellipsometry.

Sample ID	Thickness [nm]	Polar emission angle β	Ion energy E_g [keV]
6	87	$-40°$	1
7	118	$-30°$	1
8	157	$-20°$	1
9	206	$-10°$	1
10	256	0°	1
11	309	10°	1
12	371	20°	1
13	419	30°	1
14	439	40°	1
15	404	50°	1
16	323	60°	1
17	213	70°	1
18	90	80°	1

O_2^+ (32 amu), Ar^+ (40 amu), Ti^{+s} (48 amu), and TiO^+ (64 amu). The energy distributions of O^+, Ar^+, Ti^+, and TiO^+ broaden with increasing emission angle β (decreasing scattering angle γ). The same behavior is observed for simulated energy distributions using the Stopping and Range of Ions in Matter (SRIM) analyzes. The influence of the sputtering geometry on the energy of the secondary particles is depicted in Fig. 3.

Using the Tauc–Lorentz (TL) model, we get better-fitted values for all parameters of the TL-function (one parameter is E_g) and thickness. The thickness of the TiO_2 film measured by spectroscopic ellipsometry is depicted in Table I.

Data on the thickness of the TiO_2 film as a function of polar emission angle are summarized in Fig. 4a. The thickness distribution is over-cosine shape ($\beta_{max} = 40°$). This over-cosine shape is related to anisotropy effects caused by the incomplete evolution of the collision cascade inside the target [18–21]. However, the shape of the thickness distribution is not symmetric, which is related to isotropic contributions [22]. The surface energy of the samples is measured using contact angle measurements before and after UV light irradiation. In addition, there is actually a slight increase in absorption at 432 nm after implantation (Fig. 4b).

Rutherford backscattering spectrometry (RBS) measurements showed that the films are stoichiometric, i.e., the ratio Ti:O equals 1:2. Additionally, Ar particles were found inside the TiO_2 films grown by sputtering with Ar ions [14].

XRD reveals that all TiO_2 films are amorphous, while atomic force microscopy measurements show that the surface is very smooth, i.e., the root mean square (rms) roughness is $\sigma \leq 0.22$ nm. It seems to be unaffected by the ion incidence angle [14].

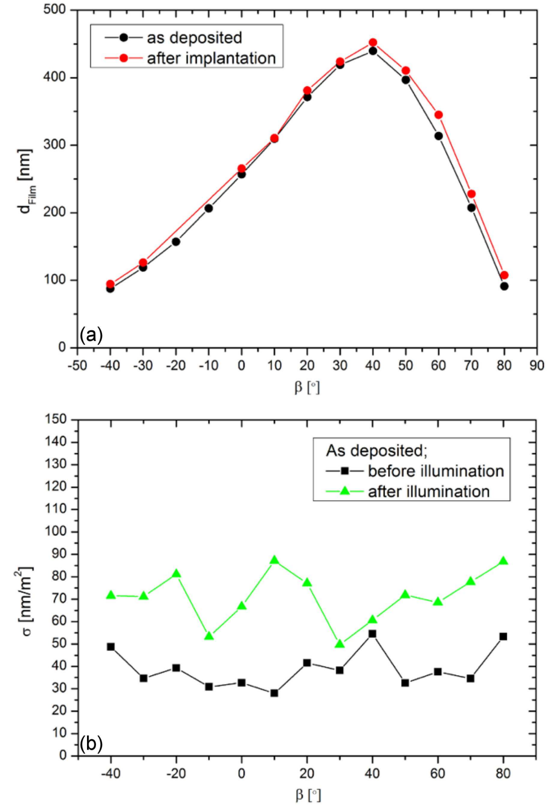

Fig. 4. Film thickness and surface energy versus polar emission angle.

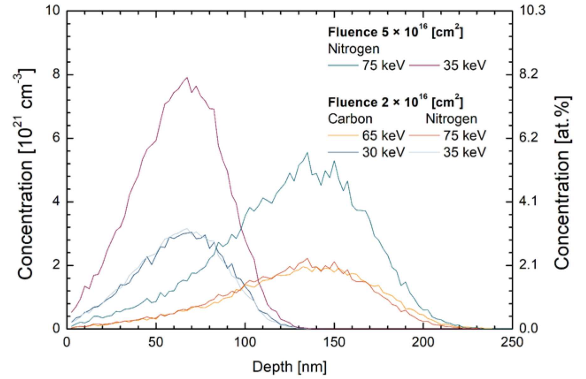

Fig. 5. Concentration profiles of carbon and nitrogen by SRIM.

The optical data of the film produced by this method is already described by the dielectric function or index of refraction; increasing the energy of the ion leads to a decrease in the index of refraction [14]. The optical properties are correlated with the film density, which is influenced by the energy of the film-forming particles.

The next experiment consisted in doping samples with carbon and nitrogen using ion implanter IMC-200. We have employed mixtures of energies/species: 65 keV C + 75 keV N, 30 keV C + 35 keV N, and 35 keV N + 75 keV N to increase the local dopant concentration and to

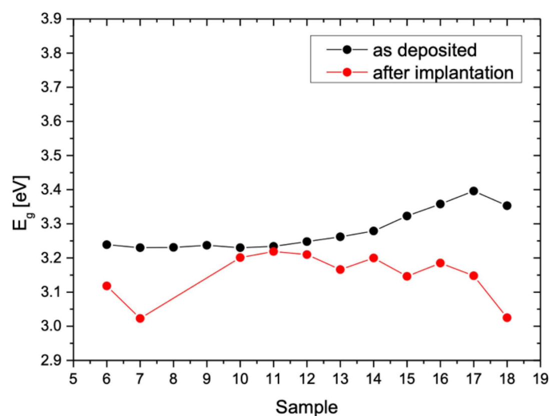

Fig. 6. Band structure of films before and after implantation.

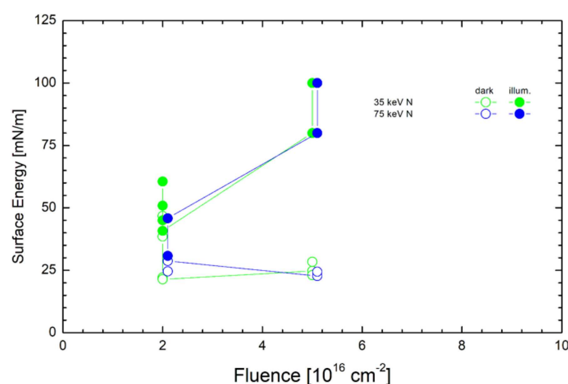

Fig. 7. Variation of surface energy with ion fluence before and after illumination.

adjust the depth to the penetration range of the light. The purpose was to investigate whether synergy effects exist for a combination of carbon and nitrogen dopants. We have combinations of fluences up to 7×10^{16} cm^{-2}, corresponding to local concentrations of up to 10 at.%. Figure 5 presents the calculated depth profiles for selected samples.

From the experimental results, one can notice that a visible change in the band structure of the deposited layers is achieved after implantation, i.e., the energy bandgap is reduced for almost all implanted samples, especially for films with smaller thicknesses as shown in Fig. 6. The effect of implantation on photoactivity is depicted in Fig. 7, which shows increasing surface energy with increasing ion fluence. In the data obtained for surface energies, the strong influence of the ion fluence on the photoactivity is observed.

4. Conclusions

Using PVD processes — ion beam sputter deposition and conventional ion implantation — the formation of photoactive TiO_2 thin films with a reduced band gap is reported.

It can be stated that the ion implantation at concentrations lower than 10 at.% can lead to increased photoactivity under UV irradiation. Reducing the bandgap by carbon and/or nitrogen implantation before changing from semiconductor to semimetal is challenging. This was known for direct co-deposition during PVD by vacuum arc, and now it was shown to be true for post-implantation after ion beam sputter deposition as well. Furthermore, the doping process increases the surface energy, which leads to improved photoactive properties. However, further work is necessary to elucidate the mechanisms and to establish whether this is doping or a damaging effect.

Acknowledgments

This study was supported by DAAD Grant, Research Stays for University Academics and Scientists, (57378441), personal ref. no.: 91656534. A.G. would like to thank Stephan Mandl as supervisor and for Raman and IMC-200 Implanter measurements, Thomas Lautenschläger for preparing IBSD samples and ESMS measurement and Carsten Bundesmann for optical data.

References

[1] W. Hofmeister, E. Tillmanns, W.H. Bauer, *Acta Crystallogr. C* **40**, 1510 (1984).

[2] A. Fujishima, K. Honda, *Nature* **238**, 37 (1972).

[3] R. Wang, K. Hashimoto, A. Fujishima, M. Chikuni, E. Kojima, A. Kitamura, M. Shimohigoshi, T. Watanabe, *Nature* **388**, 431 (1997).

[4] P. Löbl, M. Huppertz, D. Mergel, *Thin Solid Films* **251**, 72 (1994).

[5] K. Fischer, M. Kühnert, R. Gläser, A. Schulze, *RSC Adv.* **5**, 16340 (2015).

[6] J.M. Schneider, S. Rohde, W.D. Sproul, A. Matthews, *J. Phys. D. Appl. Phys.* **33**, R173 (2000).

[7] D. Manova, A. Gjevori, F. Haberkorn, J. Lutz, S. Dimitrov, J.W. Gerlach, E. Valcheva, S. Mändl, *Phys. Status Solidi A* **206**, 71 (2009).

[8] T. Morikawa, R. Asahi, T. Ohwaki, K. Aoki, Y. Taga, *Jpn. J. Appl. Phys.* **40**, L561 (2001).

[9] D.H. Lee, Y.S. Cho,W.I. Yi, T.S. Kim, J.K. Lee, H. Jin Jung, *Appl. Phys. Lett.* **66**, 815 (1995).

[10] I. Asenova, D. Manova, S. Mändl, *J. Phys. Conf. Ser.* **559**, 012008 (2014).

[11] B. Choudhury, S. Bayan, A. Choudhury, P. Chakraborty, *J. Colloid Interface Sci.* **465**, 1 (2016).

[12] S. Abu Bakar, G. Byzynski, C. Ribeiro, *J. Alloys Compd.* **666**, 38 (2016).

[13] J. Pan, S.P. Jiang, *J. Colloid Interface Sci.* **469**, 25 (2016).

[14] T. Lautenschläger, C. Bundesmann, *J. Vacuum Sci. Technol. A* **35**, 041001 (2017).

[15] C. Bundesmann, T. Lautenschläger, D. Spemann, A. Finzel, E. Thelander, M. Mensing, F. Frost, *Appl. Surf. Sci.* **421**, 331 (2017).

[16] D. Spemann, T. Reinert, J. Vogt, T. Andrea, N. Barapatre, R. Feder, A.M. Jakob, N. Liebing, C. Meinecke, F. Men-zel, M. Rothermel, T. Butz, *Nucl. Instrum. Methods Phys. Res. Sect. B* **269**, 2175 (2011).

[17] D.K. Owens, R.C. Wendt, *J. Appl. Polym. Sci.* **13(8)**, 1741 (1969).

[18] A. Goehlich, N. Niemöller, H.F. Döbele, *Phys. Rev. B* **62**, 9349 (2000).

[19] M. Stepanova, S.K. Dew, *J. Vacuum Sci. Technol. A* **19**, 2805 (2001).

[20] M. Stepanova, S.K. Dew, *J. Appl. Phys* **92**, 1699 (2002).

[21] M. Stepanova, S.K. Dew, *Method Phys. Res. Sect. B* **215**, 357 (2004).

[22] T. Lautenschläger, R. Feder, H. Neumann, C. Rice, M. Schubert, C. Bundesmann, *Nucl. Instrum. Methods Phys. Res. Sect. B* **385**, 30 (2016).